Science Advances
AAAS

Supplementary Materials for

Mad3 modulates the G_1 Cdk and acts as a timer in the Start network

Alexis P. Pérez, Marta H. Artés, David F. Moreno, Josep Clotet*, Martí Aldea*

*Corresponding author. Email: jclotet@uic.es (J.C.); marti.aldea@ibmb.csic.es (M.A.)

Published 6 May 2022, *Sci. Adv.* **8**, eabm4086 (2022)
DOI: 10.1126/sciadv.abm4086

The PDF file includes:

Figs. S1 to S5
Table S1
Legend for data file S1

Other Supplementary Material for this manuscript includes the following:

Data file S1

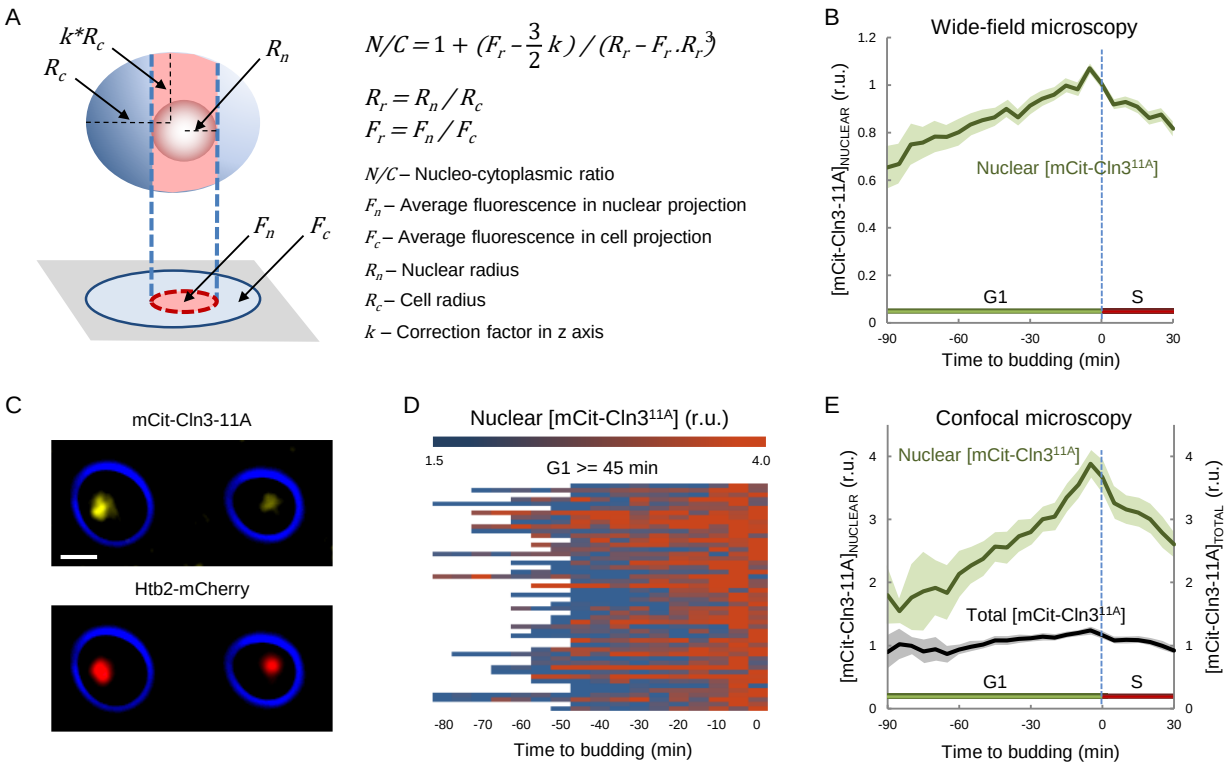

Fig. S1. Cln3^{11A} accumulates in the nucleus during G1 and reaches a maximum around Start

(A) Fluorescence within the nuclear projected area is influenced by fluorescence levels in both nuclear and cytoplasmic compartments. Briefly, the nuclear projection collects fluorescence originated from a column defined by the nuclear diameter and the cell height. Total fluorescence in the column is the weighted sum of nuclear and cytoplasmic concentrations of fluorophore assuming that the column is a cylinder and the nucleus a sphere with known dimensions relative to the cell. Cytoplasmic fluorescence (and concentration) is obtained from cell regions outside the nuclear projection, and the ratio of the nuclear to cytoplasmic concentration of the fluorescent protein is calculated as $N/C = 1 + \left(F_r - \frac{3}{2} * k\right) / (R_r - F_r * R_r^3)$, where F_r is the ratio of average fluorescence signal in nuclear (F_n) and cell (F_c) projected areas, R_r is the ratio of nuclear (R_n) and cell (R_c) radius, and k corrects for cell radius variation in the z axis, which was experimentally obtained from GFP-expressing wild-type cells.

(B) Nucleo-cytoplasmic ratio of mCit-Cln3^{11A} measured by wide-field microscopy in G1 cells as in Fig. 1A aligned to budding. Relative mean ± se values (N=100) are plotted.

(C) Cells expressing mCit-Cln3^{11A} and mCh-Htb2 were analyzed by confocal time-lapse microscopy during G1 progression and entry into the cell cycle. A representative cell at different times to budding is shown. Bar is 2 µm.

(D) Heatmap displaying nuclear concentrations of mCit-Cln3^{11A} during G1 and entry into the cell cycle. Relative data were obtained from single cells (N=50) every 5 min and aligned to budding.

(E) Cellular (total) and nuclear concentrations of mCit-Cln3^{11A} in G1 cells as in panel C aligned to budding. Relative mean ± se values (N=100) are plotted.

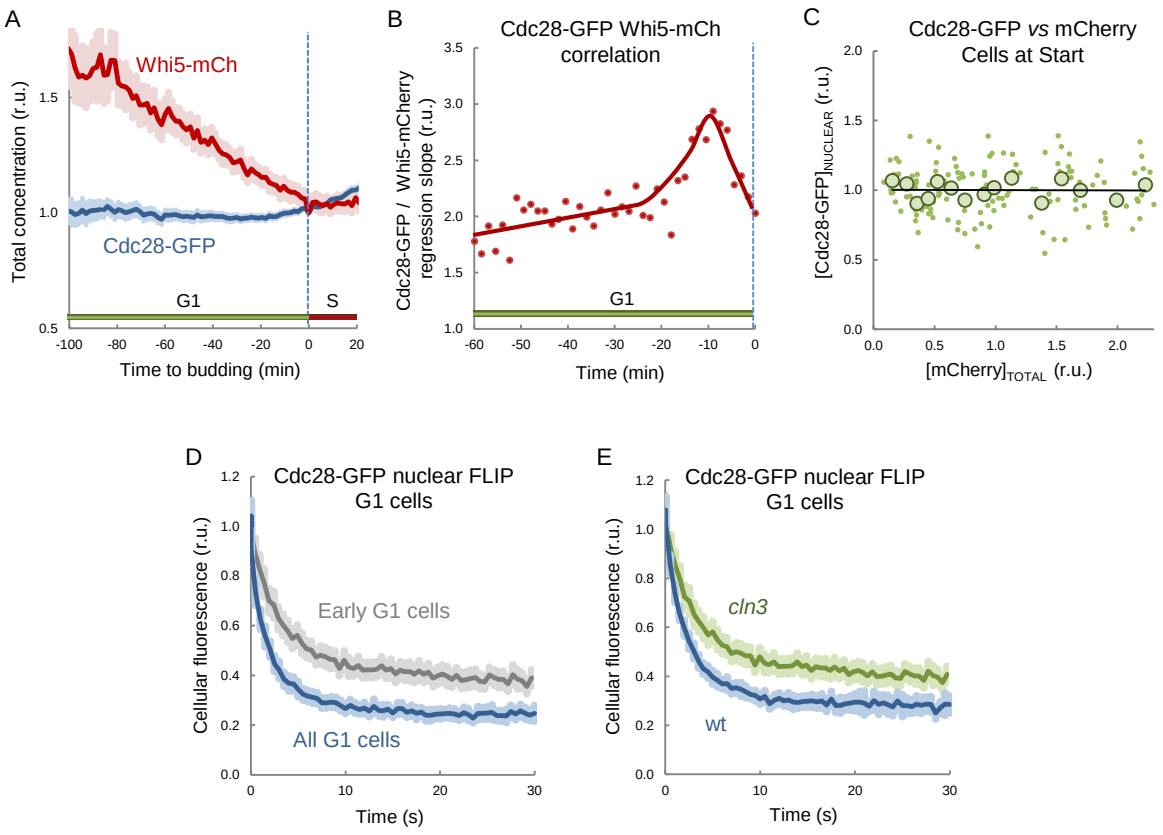

Fig. S2. Cln3 boosts nuclear import of Cdc28-GFP during cell cycle entry

(A) Cellular concentration of Cdc28-GFP and Whi5-mCh during G1 and entry into the cell cycle. Relative mean ± se values (N=100) from cells aligned to budding are plotted.

(B) Cells as in panel A were analyzed to obtain cellular Whi5-mCherry and nuclear Cdc28-GFP relative concentrations, which were used to perform linear regressions at different times during G1. Slope values and a freehand line are plotted.

(C) Nuclear Cdc28-GFP concentration as a function of cellular mCherry concentration at Start. Relative single-cell data (N=150, small circles) are plotted. Mean values of binned data (N=10, large circles) and a regression line are also shown.

(D) Total fluorescence decay of Cdc28-GFP in newborn (early G1) and cycling cells in G1 (all). Relative mean ± se values (N=100) from cells aligned to budding are plotted.

(E) Total fluorescence decay of Cdc28-GFP in wild-type (wt) and Cln3-deficient (*cln3*) cells in G1. Relative mean ± se values (N=100) from cells aligned to budding are plotted.

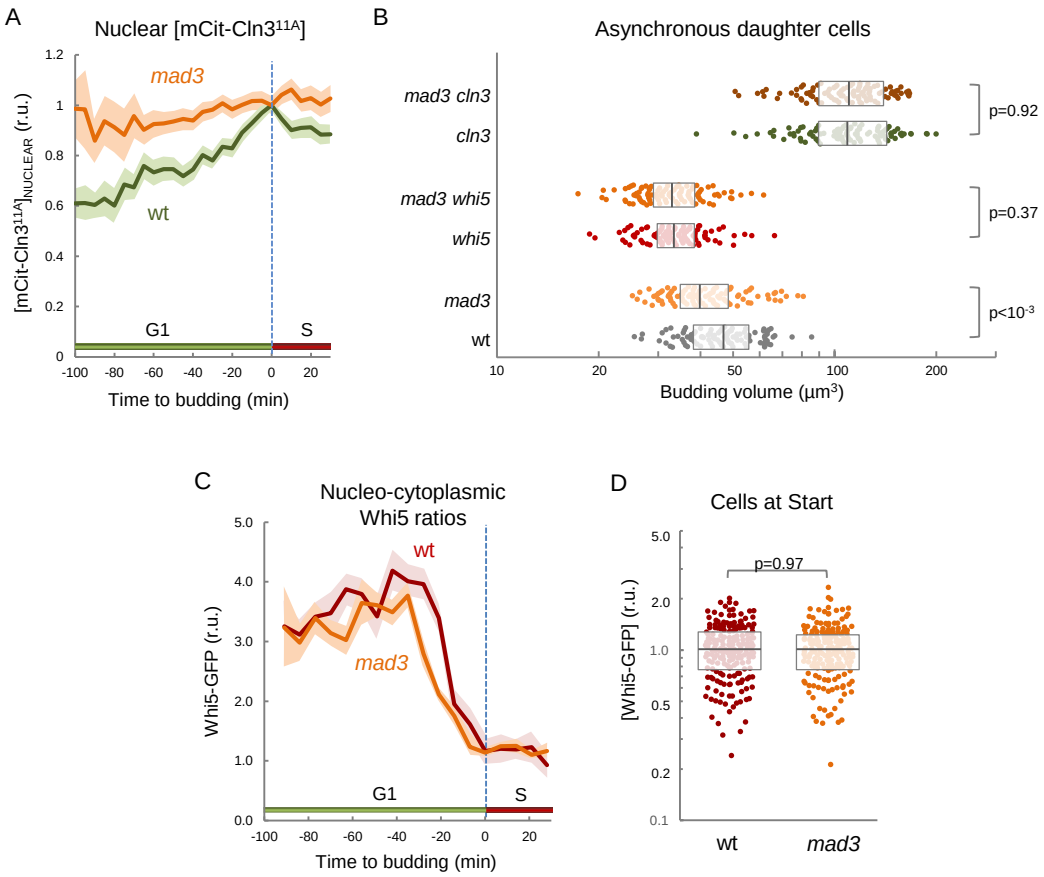

Fig. S3. Mad3 regulates Cln3 levels in G1 but does not modulate Whi5 levels at Start

(A) Nuclear concentration of mCit-Cln3^{11A} in wild-type (wt) and Mad3-deficient (*mad3*) cells aligned to budding. Mean ± se values (N=100) are plotted.

(B) Budding volume of asynchronous daughter cells with the indicated genotypes. Single-cell data with the corresponding median and quartile values are plotted. Pairwise comparisons were performed with a Mann-Whitney U test, and the resulting p-values are indicated.

(C) Nucleo-cytoplasmic Whi5-GFP ratios in wild-type (wt) and Mad3-deficient (*mad3*) cells aligned to budding. Mean ± se values (N=100) are plotted.

(D) Concentration of Whi5-GFP in wild-type (wt) and Mad3-deficient (*mad3*) G1 cells (N=100) at Start. Single-cell data with the corresponding median and quartile values are plotted. Pairwise comparisons were performed with a Mann-Whitney U test, and the resulting p-values are indicated.

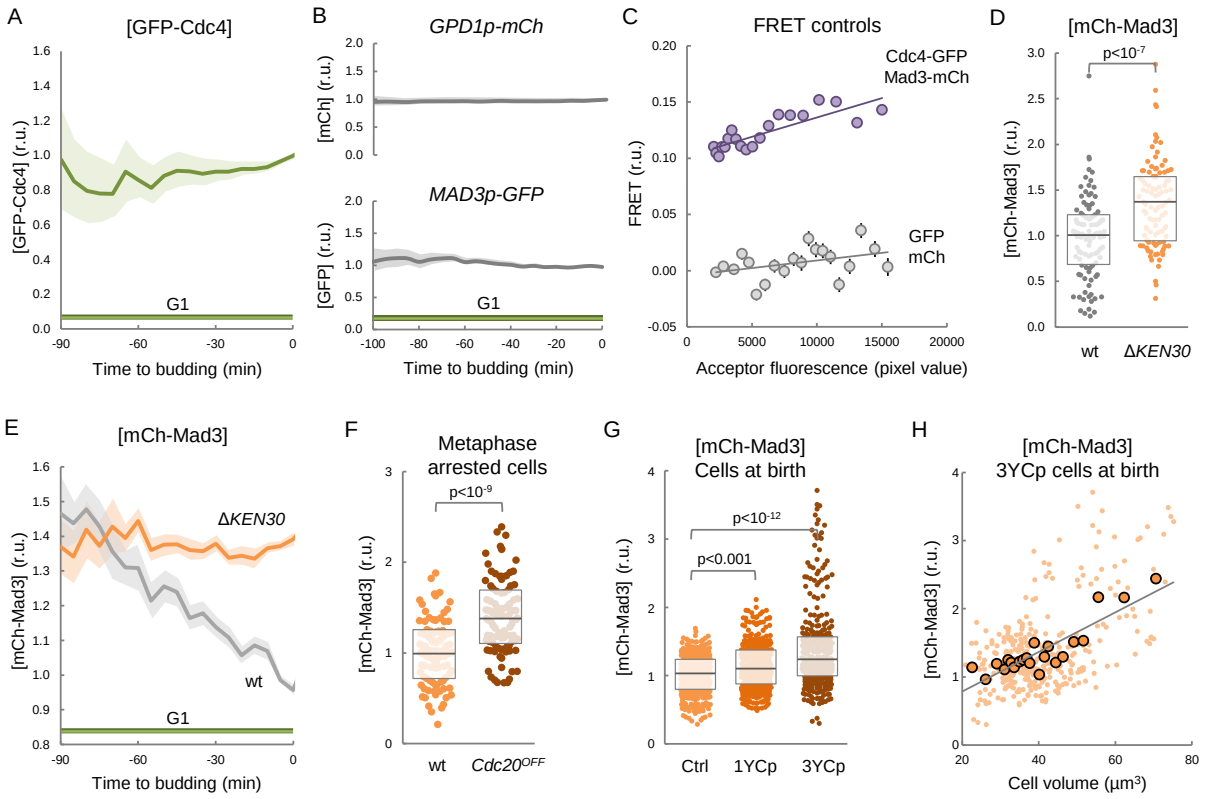

Fig. S4. Mad3 protein levels oscillate during the cell cycle as a function of APC activity

(A) Cellular concentration of GFP-Cdc4 expressed from a constitutive promoter in cycling cells aligned to budding. Relative mean ± se values (N=100) are plotted.

(B) Cellular concentration of mCherry and GFP expressed from the *GPD1p* and *MAD3p* promoters, respectively, in cycling cells aligned to budding. Relative mean ± se values (N=100) are plotted.

(C) FRET efficiencies of the GFP-Cdc4 / mCh-Mad3 and GFP / mCh pairs as a function of the acceptor (mCh) fluorescence level. Cells expressing the indicated pair of fluorescent proteins were imaged and the FRET efficiency in random pixels was calculated as described in Materials and Methods and binned by the acceptor fluorescence. Relative mean ± se values (N=1000) with the corresponding linear regression lines are plotted.

(D) Cellular concentration of mCh fused to wild-type or ΔKEN30 Mad3 proteins at budding. Single-cell data with the corresponding median and quartile values are plotted. Pairwise comparisons were performed with a Mann-Whitney U test, and the resulting p-values are indicated.

(E) Cellular concentration of mCh fused to wild-type or ΔKEN30 Mad3 proteins in cycling cells aligned to budding. Relative mean ± se values (N=100) to that of wild-type cells at budding are plotted.

(F) Concentration of mCh-Mad3 in Cdc20-arrested cells. Single-cell data with the corresponding median and quartile values are plotted. Pairwise comparisons were performed with a Mann-Whitney U test, and the resulting p-values are indicated.

(G) Concentration of mCh-Mad3 in cells at birth containing none (Ctrl), one (YCp) or three (3YCp) centromeric vectors. Single-cell data with the corresponding median and quartile values are plotted. Pairwise comparisons were performed with a Mann-Whitney U test, and the resulting p-values are indicated.

(H) Cellular concentration of mCh-Mad3 in wild-type cells at birth containing three centromeric vectors as a function of cell volume. Relative single-cell (N=300, small circles) and binned data (N=20, large circles) with the corresponding regression lines are plotted.

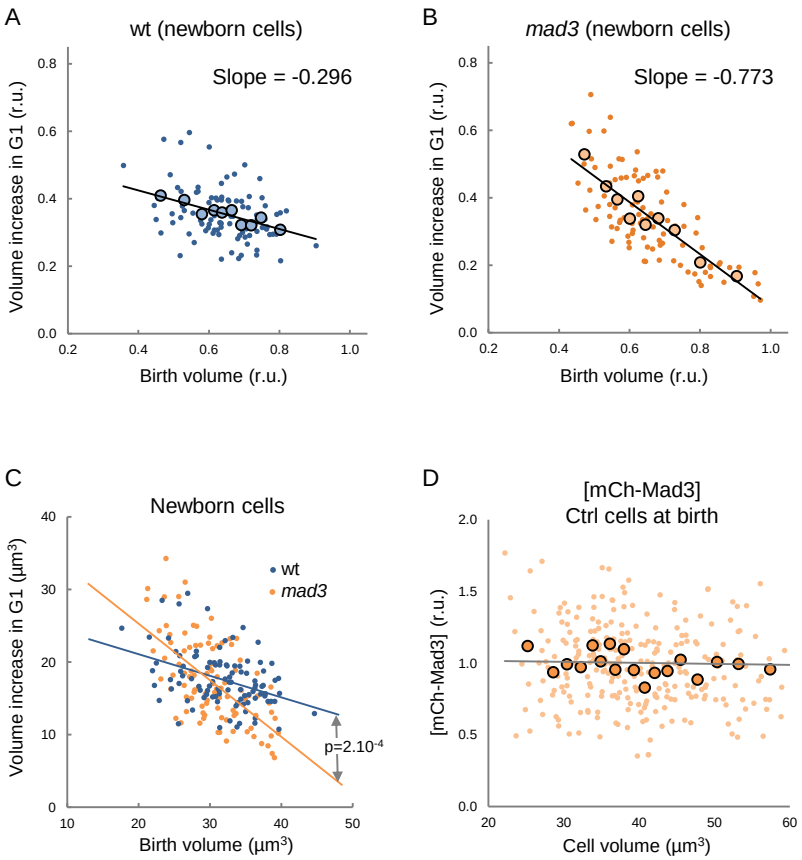

Fig. S5. Mad3 tilts the sizer behavior of G1 control

(A, B) Cell volume increase during G1 as a function of birth volume in newborn wild-type (wt, A) and Mad3-deficient (mad3, B) cells. Relative single-cell data (N=100, small circles) are plotted. Mean values of binned data (N=10, large circles) and regression lines are also shown.

(C) Single-cell data of wild-type (wt) and Mad3-deficient (mad3) cells in panels A and B are plotted in non-normalized volume units (μm^3) with the corresponding regression lines. Slopes were compared with a t test, and the resulting p value is shown.

(D) Cellular concentration of mCh-Mad3 in wild-type cells at birth as a function of cell volume. Relative single-cell (N=300, small circles) and binned data (N=20, large circles) with the corresponding regression lines are plotted.

Table S1. Yeast strains.

Strain	Source
CML128 (Mat**a** *leu2-3,112 trp1-1 ura3-52 his4-1 can1-100*)	Our lab stocks
W303-1A (Mat**a** *leu2-3,112 trp1-1 ura3-1 ade2-1 his3-11,15 can1-100*)	Our lab stocks
KSY083-5 (*mCitrine-CLN3^{11A}::NAT*)	Jan Skotheim
CYC216 (*CDC28-GFP::KAN)*	This study
CYC228 (*CDC28-GFP::KAN cln3::LEU2*)	This study
CYC457 (*CDC28-GFP::KAN HTB2-mCherry::HYG*)	This study
CYC459 (*CDC28-GFP::KAN HTB2-mCherry::HYG cln3::LEU2*)	This study
MAG714 (*whi5::KAN*)	This study
MAG1092 (*CDC28-GFP::KAN WHI5-mCherry::HYG*)	This study
MAG1334 (*mCitrine-CLN3^{11A}::NAT HTB2-mCherry::HYG*)	This study
MAG1463 (*whi5::LEU2 mad3::KAN*)	This study
MAG2013 (*mCitrine-CLN3^{11A}::NAT mad3::KAN*)	This study
MAG2458 (*TEF1p-GFP-CDC4::NAT*)	This study
MAG2501 (*GPD1p-mCherry-MAD3::KAN*)	This study
MAG2509 (*GPD1p-mCherry-MAD3::KAN TEF1p-GFP-CDC4::NAT*)	This study
MAG2510 (*mad3::KAN*)	This study
MAG2621 (*GPD1p-mCherry-MAD3::HIS3 GAL1p- CDC20::KAN*)	This study
MAG2771 (*WHI5-GFP::KAN*)	This study
MAG2773 (*WHI5-GFP::KAN mad3::HIS3*)	This study
MAG2823 (*MAD3p-GFP::HIS3)*	This study
MAG2825 (*GPD1p-mCherry::KAN*)	This study
MAG2827 (*cln3::TRP1*)	This study
MAG2829 (*cln3::TRP1 mad3::KAN*)	This study

Data S1. (separate file)

Budding volume predictions by sizer, timer, adder, timer-sizer and timer-adder models.